

Active Contours Driven by Local Gaussian Distribution Fitting and Local Robust Statistics

Xiao-Liang Jiang^{1,2,*}, Kai-Ping Feng¹, Huan Lin¹,
Jian Tang¹, Zhao-Zhong Zhou¹ and Jun Li²

¹College of Mechanical Engineering, Quzhou University,
Quzhou, Zhejiang 324000, China

²College of Mechanical Engineering, Southwest Jiaotong University
Chengdu, Sichuan 610031, China

*Corresponding author: jxl_swjtu@163.com

Received May, 2017; revised October, 2017

ABSTRACT. *Image segmentation has always been a fundamental problem in image analysis and understanding due to the intensity inhomogeneity. In order to address this issues, a novel region-based approach which combines the local Gaussian distribution fitting (LGDF) with local robust statistics is presented. In the proposed model, we integrate the local robust statistics information with the LGDF energy term which makes use of the inter-quartile range, mean absolute deviation and intensity median in local region. Moreover, the penalty energy term is incorporated into the energy function to avoid the re-initialization. Finally, minimization of this energy function with a level set regularization term. Experiments on images of various modalities demonstrated the superior performance of the proposed method when compared with other state-of-the-art approaches.*

Keywords: Image segmentation, Intensity inhomogeneity, Local Gaussian distribution fitting, Local robust statistics

1. Introduction. Image segmentation has always been a crucial step in image understanding and computer vision. In recent years, scholars have provided a large body of image segmentation algorithms, one of the most attractive methods is active contour model (ACM) [1] which has been widely applied. The essential idea of ACM is to obtain the target boundaries according to an energy-minimizing method. Existing active contour models can be generally categorized into two major groups: edge-based models [2-6] and region-based models [7-11].

Edge-based models often utilize an edge indicator to stop the curve from the target boundaries. They have been successfully used to extract contour of a large gradient, but it is sensitive to discontinuous boundaries and noise. Region-based models usually use a certain region descriptor to find a partition on the image field. Therefore, they show better performance on images with weak boundaries. The Chan-Vese (C-V) model, presented by Chan and Vese [12], is one of the most common region-based models. Nevertheless, this method cannot segment the images with intensity inhomogeneity because it supposes that the grayscale of image are statistically homogeneous.

Recently, local intensity information is applied to handle intensity inhomogeneity. For example, Li et al. [13-14] presented a method driven by region scalable fitting energy which is known as the local binary fitting (LBF) model. This model introduced the

intensity information of local region based variational level set approach. Thus, it can segment the images with intensity non-uniformity. However, when the initial contour is set inappropriately, it is easy to fall into local minimum. In [15], Zhang et al. presented another local active contour model with local Gaussian distribution fitting (LGDF) energy. This approach used the Gaussian distribution with spatially varying mean and variance to describe the image model. Thereby it can distinguish regions with similar intensity means but different variances. In [16], Li et al. think that only utilizing intensity information may have effects on convergence rate, thus they presented a novel region-based model with local statistics information, named NRBLSI model. So the method can be used for accurate segmentation of medical images in the presence of severe intensity inhomogeneity. However, all of them are sensitive to initialization of the contour to some extent.

In this study, we propose a novel LGDF model with local robust statistics information. As is pointed out in [17], the popular characteristic of the local robust statistics is that they are not sensitive to image noise and they can compute efficiently. By integrating the local robust statistics information, the new LGDF model can make use of the inter-quartile range, mean absolute deviation and intensity median in local region. Some experiments have been conducted on images of various modalities to demonstrate the superiority of our model when compared with the LBF, NRBLSI and LGDF model.

The rest of this paper is organized as follows. In Section 2, we briefly review some related works. Section 3 focuses on our method. In Section 4, the proposed model is validated by experiments on several synthetic and real images. Finally, we summarize our work in the last Section.

2. Background.

2.1. C-V model. Let $I : \Omega \rightarrow R$ be an original image and C be a closed curve. Chan and Vese [12] presented a common region-based method based on Mumford-Shah model [18], the energy functional is presented as follows:

$$E^{CV}(C, c_1, c_2) = \lambda_1 \int_{inside(C)} |I(x) - c_1|^2 dx + \lambda_2 \int_{outside(C)} |I(x) - c_2|^2 dx + \nu |C| \quad (1)$$

where $\lambda_1, \lambda_2, \nu$ are positive constants, c_1 and c_2 denote the grey value inside and outside the contour C . The first and second are the data term that drive curve to approach the boundaries of object, $|C|$ is the length term. Because the grayscale of image are statistically homogeneous, C-V model cannot segment the images with intensity inhomogeneity.

2.2. LBF model. In order to overcome the problem of intensity inhomogeneity, Li et al. [13-14] introduced a variational level set approach driven by region scalable fitting energy. The method is based on the following model:

$$E^{LBF}(C, f_1, f_2) = \lambda_1 \int_{\Omega} \int_{inside(C)} K_{\sigma}(x - y) |I(y) - f_1(x)|^2 dy dx + \lambda_2 \int_{\Omega} \int_{outside(C)} K_{\sigma}(x - y) |I(y) - f_2(x)|^2 dy dx \quad (2)$$

where K_{σ} is a truncated Gaussian kernel where $K(x - y) = 0$ for $|x - y| \geq r$. f_1 and f_2 are two smooth functions in a Gaussian window, respectively. Thus, LBF model has the capability of handling intensity inhomogeneity. However, if the initial contour is set inappropriately, it is easy to fall into local minimum.

2.3. LGDF model. In [15], Zhang et al. presented a statistical and variational level set method. By using maximum a posteriori probability and Bayes' rule, the LGDF energy can be described as follows:

$$E^{LGDF} = \int_{\Omega} \left(\sum_{i=1}^2 \lambda_i \int_{\Omega_i} -\omega(x-y) \log p_{i,x}(I(y)) dy \right) dx \quad (3)$$

where λ_i are the positive constant and the $p_{i,x}(I(y))$ is the probability density in region $\Omega_x \cap \Omega_i$, which is defined as:

$$p_{i,x}(I(y)) = \frac{1}{\sqrt{2\pi}\sigma_i(x)} \exp\left(-\frac{(\mu_i(x) - I(y))^2}{2\sigma_i^2(x)}\right), i = 1, 2 \quad (4)$$

where $\mu_i(x)$ is the local intensity in the partition, $\sigma_i(x)$ is the standard deviations. Assuming that the mean and variance of the local Gaussian distribution are spatially varying parameters, thereby it can distinguish regions with similar intensity means but different variances. However, the LGDF model still has the shortcoming that the convergence rate of the curve is slow.

3. The Proposed Scheme.

3.1. Local robust statistics. As is mentioned in literature [19], the robust statistical method has been widely used in every field and it maybe has good robustness for noise and intensity inhomogeneity. The algorithm process is described as follows. First, we select a pixel x and its neighborhood in original image I . Second, in the selected neighborhood of x , their intensity values of the pixels are expressed in an increasing number x_1, x_2, \dots, x_n . Subsequently, the inter-quartile range $IQR(x)$, mean absolute deviation $MAD(x)$ and intensity median $MED(x)$ can be described as follows:

$$MED(x) = \begin{cases} x_{(n+1)/2}, & \text{if } n \text{ is odd number} \\ \frac{1}{2}[x_{n/2} + x_{(n+1)/2}], & \text{if } n \text{ is even number} \end{cases} \quad (5)$$

$$IQR(x) = Q_3(x) - Q_1(x) \quad (6)$$

$$MAD(x) = \frac{\sum_{i=1}^n |x_i - \bar{x}|}{n} \quad (7)$$

Look at Eq. (6), x_1, x_2, \dots, x_n are fell into four equal partitions, $Q_1(x)$ and $Q_3(x)$ are the first and third quartiles. \bar{x} in Eq. (7) denotes the mean of x_1, x_2, \dots, x_n . $IQR(x)$ and $MAD(x)$ are used to sharpen target boundaries, while $MED(x)$ performs well on reducing image noise. Hence, the new image can be rewritten:

$$I_{new}(x) = MED(x) + \tau_1 IQR(x) + \tau_2 MAD(x) \quad (8)$$

where τ_1 and τ_2 are information fusion coefficients. In general, the values of τ_1 and τ_2 range from 0 to 1.

3.2. Level set formulation. As is mentioned above, the energy E^{LGDF} presented in Eq. (3) is unable to fully use image information. Consequently, the LGDF model has a slow convergence rate and it is sensitive to strong noise. In order to address these problems, we propose a novel LGDF model with local robust statistics information.

In this paper, the grey value of original image I is replaced by the new input image $I_{new}(x)$. Hence, the new energy functional is expressed as follow:

$$E_{new}^{LGDF} = \int_{\Omega} \left(\sum_{i=1}^2 \lambda_i \int_{\Omega_i} -\omega(x-y) \log p_{i,x}(MED(y) + \tau_1 IQR(y) + \tau_2 MAD(y)) dy \right) dx \quad (9)$$

where λ_1 and λ_2 are positive constants.

Using the Heaviside function $H(\phi)$, the energy in Eq. (9) can be written as the following level set formulation:

$$E_{new}^{LGDF} = \int_{\Omega} \left(\sum_{i=1}^2 \lambda_i \int_{\Omega} -\omega(x-y) \log p_{i,x}(MED(y) + \tau_1 IQR(y) + \tau_2 MAD(y)) M_i(\phi(y)) dy \right) dx \quad (10)$$

where $M_1(\phi) = H(\phi)$ and $M_2(\phi) = 1 - H(\phi)$.

To derive an accurate and smooth contour, we need to add a length term $L(\phi)$ and a regularization term $P(\phi)$.

$$L(\phi) = \int_{\Omega} (|\nabla H(\phi(x))|) dx \quad (11)$$

$$P(\phi) = \int_{\Omega} \frac{1}{2} (|\nabla \phi(x)| - 1)^2 dx \quad (12)$$

Therefore the entire energy functional is

$$F_{new}^{LGDF}(\phi, \mu_1, \mu_2, \sigma_1^2, \sigma_2^2) = E_{new}^{LGDF}(\phi, \mu_1, \mu_2, \sigma_1^2, \sigma_2^2) + \mu P(\phi) + \nu L(\phi) \quad (13)$$

In our implementation, Heaviside function H is usually approximated by a smoothing function H_{ε} defined by

$$H_{\varepsilon}(x) = \frac{1}{2} \left(1 + \frac{2}{\pi} \arctan\left(\frac{x}{\varepsilon}\right) \right) \quad (14)$$

The derivative of H_{ε} is the following smoothing function:

$$\delta_{\varepsilon}(x) = \frac{1}{\pi} \frac{\varepsilon}{\varepsilon^2 + x^2} \quad (15)$$

Therefore, the energy functional F_{new}^{LGDF} in Eq. (13) is approximated by:

$$F_{new,\varepsilon}^{LGDF}(\phi, \mu_1, \mu_2, \sigma_1^2, \sigma_2^2) = E_{new,\varepsilon}^{LGDF}(\phi, \mu_1, \mu_2, \sigma_1^2, \sigma_2^2) + \mu P(\phi) + \nu L_{\varepsilon}(\phi) \quad (16)$$

3.3. Gradient descent flow. By minimization of the energy $F_{new,\varepsilon}^{LGDF}$ in (16), image segmentation can be simultaneously achieved. For fixed μ_i and σ_i , we minimize the function $F_{new,\varepsilon}^{LGDF}$ with respect to ϕ can be obtained by solving the following gradient flow equation.

$$\frac{\partial \phi}{\partial t} = -\delta_{\varepsilon}(\phi) (\lambda_1 e_1 - \lambda_2 e_2) + \mu (\Delta \phi - \operatorname{div}\left(\frac{\Delta \phi}{|\Delta \phi|}\right)) + \nu \delta_{\varepsilon}(\phi) \operatorname{div}\left(\frac{\Delta \phi}{|\Delta \phi|}\right) \quad (17)$$

where

$$e_1(x) = \int_{\Omega} \omega(x-y) \left[\log(\sqrt{2\pi}\sigma_1(y)) + \frac{(\mu_1(y) - I_{new}(x))^2}{2\sigma_1(y)^2} \right] dy \quad (18)$$

$$e_2(x) = \int_{\Omega} \omega(x-y) \left[\log(\sqrt{2\pi}\sigma_2(y)) + \frac{(\mu_2(y) - I_{new}(x))^2}{2\sigma_2(y)^2} \right] dy \quad (19)$$

By calculus of variations, the parameters $\mu_i(x)$ and $\sigma_i^2(x)$ can be expressed as:

$$\mu_i(x) = \frac{\int \omega(x-y)I_{new}(y)M_{i,\varepsilon}(\phi(y))dy}{\int \omega(x-y)M_{i,\varepsilon}(\phi(y))dy} \quad (20)$$

and

$$\sigma_i^2(x) = \frac{\int \omega(x-y)(\mu_i(x) - I_{new}(y))^2 M_{i,\varepsilon}(\phi(y))dy}{\int \omega(x-y)M_{i,\varepsilon}(\phi(y))dy} \quad (21)$$

4. Experimental Results. In this subsection, the LBF model [13-14], LGDF model [15], NRBLSI model [16], and the method of this paper are applied on a variety of synthetic images and medical images. All of the experimental results are obtained by the computer with Pentium (R) Dual-Core 2.93 GHz CPU, 4 GB RAM and Windows 7 (64 bit) operating system. Unless otherwise stated, the following default setting of the parameter is used in the experiments: $c_0 = 2.0$, scale parameter $\sigma = 3.0$, time step $\Delta t = 0.1$, $\mu = 1.0$.

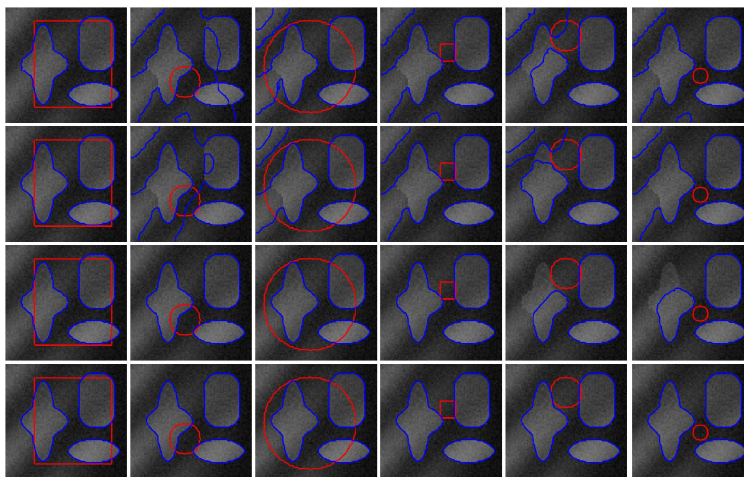


FIGURE 1. Comparison of different methods for synthetic images with different initial contours. The first row: results of LBF model. The second row: results of NRBLSI model. The third row: results of LGDF model. The last row: results of our method.

4.1. Segmentation of synthetic images. We firstly apply our method to segment two synthetic images, which are displayed in Fig. 1 and Fig. 2. The two image sizes are 79×75 and 127×96 , respectively. These images are corrupted by intensity inhomogeneity and strong noise in different levels. As shown in Fig. 1, the final segmentation results obtained after the convergence of these algorithms are marked as blue contours. First to fourth rows show the segmentation results by LBF, NRBLSI, LGDF and our method, respectively. It can be seen from Fig. 1 that our method can achieve the desirable results with different initial contours. The state of Fig. 2 is similar to Fig. 1. Both two experiments demonstrate our method is very robust to the initial contours.

4.2. Segmentation of medical images. We also evaluate the performance of our model on six medical images with obvious intensity inhomogeneity and high noise. Fig. 3 shows the segmentation results by LBF model (first row), NRBLSI model (second row), LGDF model (third row) and the proposed model (last row). The parameters are set as follows: $\lambda_1 = 1.0$, $\lambda_2 = 1.03$, $\nu = 0.001 \times 255^2$, $\tau_1 = \tau_2 = 0.1$ in our model. If $\lambda_1 < \lambda_2$

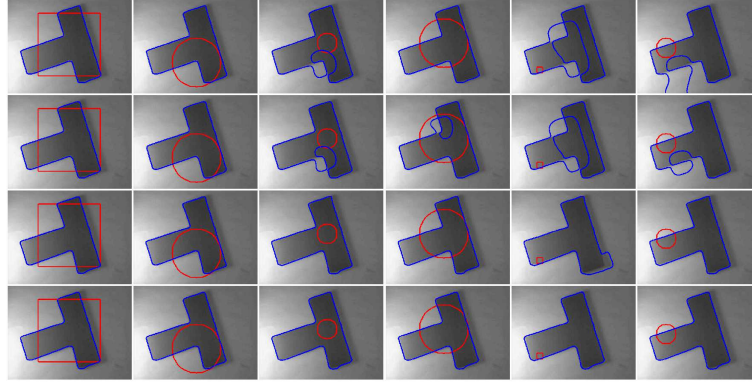


FIGURE 2. Comparison of different methods for T-shaped Images with different initial contours. The first row: results of LBF model. The second row: results of NRBLSI model. The third row: results of LGDF model. The last row: results of our method.

, the contour tends to deflate, otherwise tends to inflate. It is obvious that LBF and NRBLSI which only use the local intensity means fail to segment some medical images with intensity inhomogeneity and weak boundaries. Taking more statistical characteristics into account, LGDF model yields similar visual quality as our model in some images.

In order to test the performance of our model, the computational time and iterations for segmentation are presented in Table 1. Owing to the application of local robust statistics, the computational time and iteration number are reduced to a great extent. Experiments have proved that our method has higher computing efficiency beside the accurate segmentation.

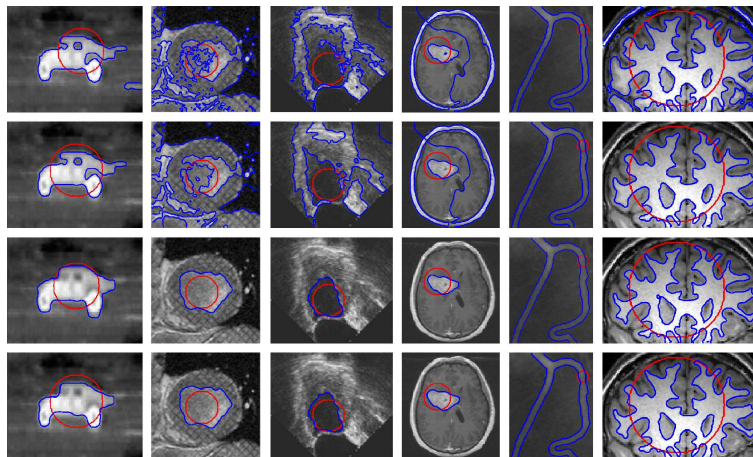


FIGURE 3. Comparison of different methods for medical images. The first row: results of LBF model. The second row: results of NRBLSI model. The third row: results of LGDF model. The last row: results of our method.

4.3. Segmentation of noise images. In order to evaluate the sensitivity to noise, we apply our method to the images corrupted by intensity inhomogeneity and noise simultaneously. In this experiment, the images with salt and pepper noise levels $\{0.01, 0.05, 0.1, 0.2, 0.3\}$ is added into original image, as shown in the first row of Fig. 4 and Fig. 5. Second to fifth rows show the segmentation result by LBF model (first row), NRBLSI model (second row), LGDF model (third row) and the proposed model (last row). We

TABLE 1. Comparison with iterations and computational time (s) for the images in Fig. 3 in the same order.

Image	LBF model		NRBLSI model		LGDF model		Our method	
	Iterations	Time	Iterations	Time	Iterations	Time	Iterations	Time
1	500	5.85	500	5.71	300	5.74	230	4.34
2	500	13.51	500	12.89	300	7.19	150	3.61
3	500	9.47	500	9.03	220	4.30	120	3.80
4	500	10.67	500	11.39	80	2.40	60	1.87
5	320	3.84	340	4.56	380	8.18	180	4.03
6	500	11.65	200	4.06	260	4.71	180	3.43

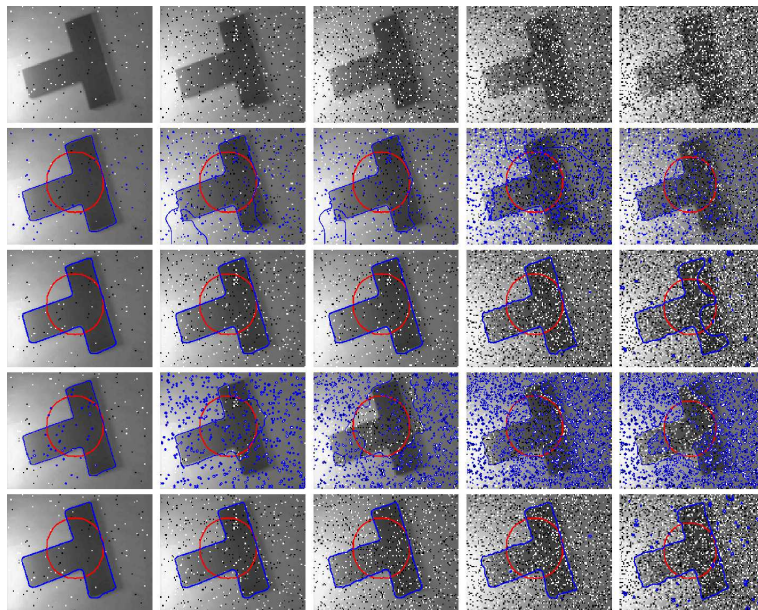


FIGURE 4. Comparison results for T-shaped image polluted by various levels of Salt and Pepper noise. The first row shows the images with noise levels $\{0.01, 0.05, 0.1, 0.2, 0.3\}$, respectively. Second to fifth rows show the segmentation result by LBF, NRBLSI, LGDF and the method.

observe from Fig. 4 and Fig. 5 that LBF and LGDF are sensitive to salt and pepper noise, and thus they get undesirable results. The reason is that, compared with LBF and LGDF, our method and NRBLSI model both contain the robust statistics information. Among the robust statistics, the intensity median is used to reduce noise. Below the noise level 0.2, NRBLSI has the capability of extracting the target polluted by salt and pepper noise to some extent. Nevertheless, when the noise density reaches to 0.3, NRBLSI cannot achieve the accuracy boundaries. By contrast, our model still can extract the boundary of object correctly under the noise level 0.3. Therefore, the robustness of our method to handle the images with salt and pepper noise is superior to the other three models.

In the next experiment, Fig. 6 and Fig. 7 show the comparison of results between our method and the other three models on images polluted by Gaussian noise. The noise level is $\{0.0005, 0.001, 0.002, 0.005\}$, respectively. We observe from Fig. 6 and Fig. 7 that all of the above models can obtain the accuracy boundary when segmenting the image with noise level 0.0005. However, when the noise level increases to 0.001, LBF and NRBLSI cannot obtain the satisfactory results. The LGDF model successfully extracts the object when images are corrupted by noise of lower strength, while our model still can detect the accuracy object boundaries. These two experiments demonstrate that the proposed

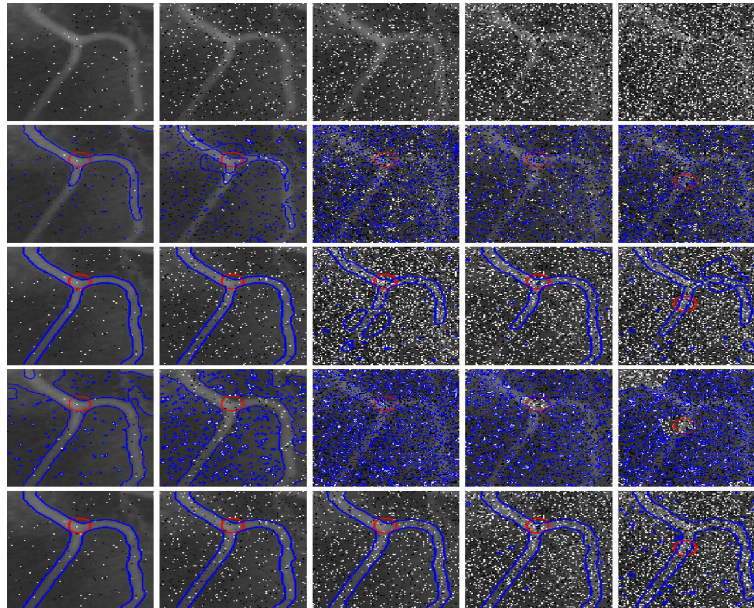


FIGURE 5. Comparison results for vessel image polluted by various levels of Salt and Pepper noise. The first row shows the images with noise levels $\{0.01, 0.05, 0.1, 0.2, 0.3\}$, respectively. Second to fifth rows show the segmentation result by LBF, NRBSI, LGDF and the method.

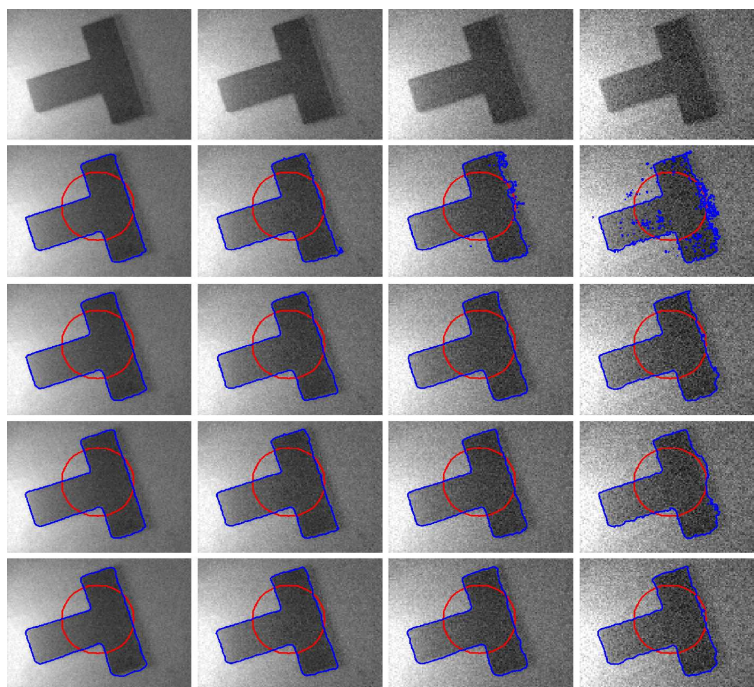


FIGURE 6. Comparison results for T-shaped image polluted by various levels of Gaussian noise. The first row shows the images with noise levels $\{0.0005, 0.001, 0.002, 0.005\}$, respectively. Second to fifth rows show the segmentation result by LBF, NRBSI, LGDF and the method.

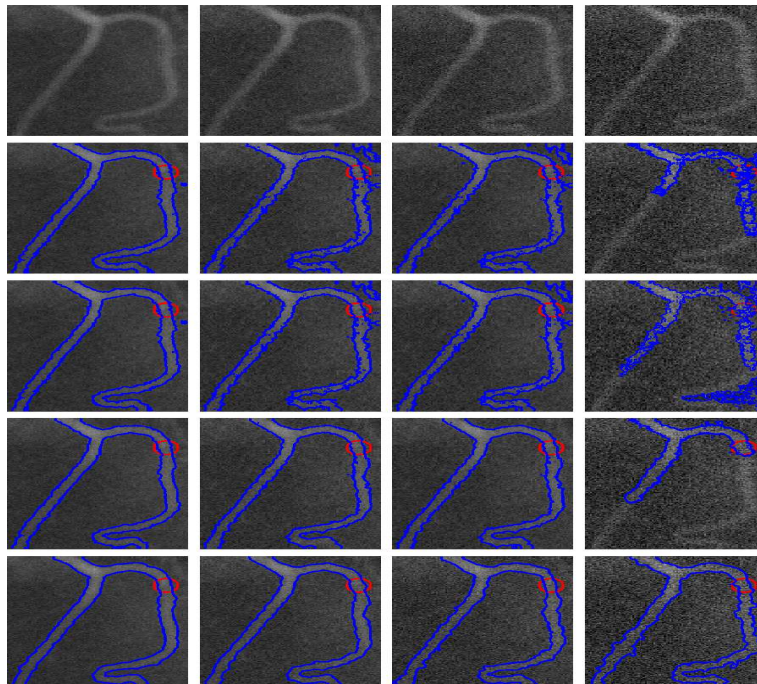


FIGURE 7. Comparison results for vessel image polluted by various levels of Gaussian noise. The first row shows the images with noise levels $\{0.0005, 0.001, 0.002, 0.005\}$, respectively. Second to fifth rows show the segmentation result by LBF, NRBLSI, LGDF and the method.

model has a good robustness to Gaussian noise.

5. Conclusions.

In this paper, we propose a novel LGDF model with local robust statistics information. In the proposed model, we efficiently utilize the advantages of local robust statistics of image, which can contribute to decreasing the effects of noise and outliers, and reducing the sensitivity to initial contour. As a result, our method has the capability of segmenting images with intensity inhomogeneity and various type of noise. The experimental results on synthetic and medical images show the superiority of our method over several state-of-the-art active contour models.

Acknowledgment.

This work is supported by the National Natural Science Foundation of China (No.51275272, 51605253), Zhejiang Provincial Natural Science Foundation of China (No.LY16E050011, LQ17C160001,LQ18F010007), Provincial Public-benefit Technology Application Research of Zhejiang (No. 2017C37082, 2016C37058, 2016C31127), Key Laboratory of Air-driven Equipment Technology of Zhejiang Province(No.2018E10011).

REFERENCES

- [1] M. Kass, A. Witkin, and D. Terzopoulos, Snakes: active contour models, *International Journal of Computer Vision*, vol. 1, no. 4, pp. 321-331, 1988.
- [2] M. Ciecholewski, An edge-based active contour model using an inflation/deflation force with a damping coefficient, *Expert Systems with Applications*, vol. 44(C), pp. 22-36, 2016.
- [3] A. Pratondo, C. K. Chui, and S. H. Ong, Robust edge-stop functions for edge-based active contour models in medical image segmentation, *IEEE Signal Processing Letters*, vol. 23, no. 2, pp. 222-226, 2016.

- [4] A. H. Foruzan, and Y. W. Chen, Improved segmentation of low-contrast lesions using sigmoid edge model, *International Journal of Computer Assisted Radiology and Surgery*, vol. 11, no. 7, pp. 1267-1283, 2016.
- [5] D. Gupta, and R. S. Anand, A hybrid edge-based segmentation approach for ultrasound medical images, *Biomedical Signal Processing and Control*, vol. 31, pp. 116-126, 2017.
- [6] C. Liu, W. Liu, and W. Xing, An improved edge-based level set method combining local regional fitting information for noisy image segmentation, *Signal Processing*, vol. 130, pp. 12-21, 2017.
- [7] S. Niu, Q. Chen, L. D. Sisternes, Z. Ji, Z. Zhou, and D. L. Rubin, Robust noise region-based active contour model via local similarity factor for image segmentation, *Pattern Recognition*, vol. 61, pp. 104-119, 2016.
- [8] T. D. Bui, C. Ahn, and J. Shin, Unsupervised segmentation of noisy and inhomogeneous images using global region statistics with non-convex regularization, *Digital Signal Processing*, vol. 57, pp. 13-33, 2016.
- [9] G. Wang, Q. Dong, Z. Pan, W. Zhang, J. Duan, L. Bai, and G. P. Zhang, Retinex theory based active contour model for segmentation of inhomogeneous images, *Digital Signal Processing*, vol. 50(C), pp. 43-50, 2016.
- [10] Q. Liu, M. Jiang, P. Bai, and G. Yang, A novel level set model with automated initialization and controlling parameters for medical image segmentation, *Computerized Medical Imaging and Graphics*, vol. 48, pp. 21-29, 2015.
- [11] H. Bakir, M. Charfi, and J. Zrida, Automatic active contour segmentation approach via vector field convolution, *Signal, Image and Video Processing*, vol. 10, no. 1, pp. 1-10, 2016.
- [12] T. F. Chan, and L. A. Vese, Active contours without edges, *IEEE Transactions on Image Processing*, vol. 10, no. 2, pp. 266-277, 2001.
- [13] C. M. Li, C. Y. Kao, J. C. Gore, and Z. H. Ding, Implicit active contours driven by local binary fitting energy, *in: Proceeding of CVPR'07*, 2007, pp. 1-7.
- [14] C. M. Li, C. Y. Kao, J. C. Gore, and Z. H. Ding, Minimization of region-scalable fitting energy for image segmentation, *IEEE Transactions on Image Processing*, vol. 17, no. 10, pp. 1940-1949, 2008.
- [15] C. Li and W. Li, Active contour driven by local Gaussian distribution fitting energy, *Signal processing*, vol. 89, no. 12, pp.2435-2447, 2009.
- [16] L.S. Li and L. Zeng, Segmentation of computer tomography image using local robust statistics and region-scalable fitting, *Journal of X-Ray Science and Technology*, vol. 20, no. 3, pp.255-267, 2012.
- [17] C. Huang and L. Zeng, Robust image segmentation using local robust statistics and correntropy-based K-means clustering, *Optics and Lasers in Engineering*, vol. 66, pp.187-203, 2015.
- [18] D. Mumford, and J. Shah, Optimal approximation by piecewise smooth function and associated variational problems, *Communications on Pure and Applied Mathematics*, vol. 42, no. 5, pp. 577C685, 1989.
- [19] E. Pichon, A Tannenbaum and R. Kikinis, A statistically based flow for image segmentation, *Medical Image Analysis*, vol. 8, no. 3, pp. 267C274, 2004.